Materials Today Communications 15 (2018) 254–259

Contents lists available at ScienceDirect

Materials Today Communications

journal homepage: www.elsevier.com/locate/mtcomm

Design, fabrication and testing of discrete 3D sand-printed floor prototypes

M. Rippmann*, A. Liew, T. Van Mele, P. Block

Block Research Group, Institute of technology in Architecture, ETH Zurich, Switzerland

ARTICLE INFO

Keywords:
3D printing
Additive manufacturing
Floor
Prototype
Funicular
Compression
Arch
Sand
Unreinforced
Vault

ABSTRACT

This paper describes the concept, design, fabrication and experimental testing of prototype 3D sand-printed floors, derived from principles of shallow arching action and discrete structural systems to initiate internal compressive stresses rather than exclusively flexural stresses. Using industrial 3D printing with silica sand, the presented system enables significant weight reduction of up to 70% when compared to conventional concrete floor slabs, by placing the 3D printed material in key structural areas and by externalising tension forces. The form-finding process for the global shape of the floors and the generation of structurally optimised print mesh geometries are presented. Three floor prototypes with varying rib geometries and discretisation layouts were studied. The results from the serviceability and ultimate load testing of the floors are documented in detail. The data showed that this relatively weak material can be used, without internal reinforcement, to print a floor that is able to support loads in excess of typical design code levels.

1. Introduction

This research describes a series of pre-fabricated and segmented floors, fabricated using 3D sand printing. The structural principle of the vaulted rib-stiffened floor system is based on shallow arching action to initiate compressive stresses rather than exclusively flexural normal stresses, leading to lightweight and stiff structures. Resulting horizontal thrusts can be taken either by ties or horizontal restraints at the supports. The ribs allow a floor plate to be supported on the topside by transmitting the loads to the vault, as well as stiffening the structure, the latter of which is important for resisting asymmetric loading (Fig. 1). The concept stems from traditional thin-tile compression vaults stiffened by diaphragms or ribs, developed in the 19th century [1].

The presented system enables a significant weight reduction of up to 70% when compared to conventional solid concrete floor slabs by placing material in key structural areas. The potential impact of such material savings is evident, considering that, due to its extensive use, concrete is the material that globally contains the greatest amount of anthropogenic carbon dioxide [2], and that concrete floor systems and roof structures contribute greatest to the material quantities used in building structures [3]. Previous research has demonstrated the structural feasibility of using a thin-vaulted, rib-stiffened concrete floor without traditional reinforcement bars to build strong and stiff structures with low mass [4]. However, the fabrication of lightweight concrete floors with complex rib geometries can be expensive, due to the requirement of custom CNC-milled formwork moulds. This is particularly problematic for non-repetitive floor elements with varying design parameters such as size, shape and design load.

In contrast, additive manufacturing processes are perfectly suited to produce bespoke structural elements without additional costs for non-repetitive part geometries. In particular, 3D printing based on binder jetting [5–7] and 3D printing by layered extrusion [8,9] have been used at larger scales to produce building parts with intricate geometries in architecture and construction. However, due to the layered manufacturing and bonding process, the resulting materials have typically low tensile and flexural capacity [10], making them undesirable for many structural applications in construction. Currently, for most building components, the use of such additive manufacturing techniques requires additional stiffening, as for example, through filling hollow 3D printed parts with ultra-high performance concrete [11], and more importantly, a strategy to introduce reinforcement bars. The goal of this research project was to employ structural systems that work predominantly in compression, making use of the higher compressive strength of 3D printed materials.

This research paper is laid out as follows: Section 2 describes the geometry of the floor prototypes, including an outline of the form-finding process and a description of the subsequent mesh generation for 3D printing. Section 3 details the material properties from experimental testing of 3D printed specimens. Section 4 describes the experimental setup used in the service and ultimate load testing for three floors. Section 5 discusses the environmental impact and resource efficiency of the proposed floor system. Finally, conclusions are drawn in Section 6.

* Corresponding author.
E-mail address: rippmann@arch.ethz.ch (M. Rippmann).

https://doi.org/10.1016/j.mtcomm.2018.03.005
Received 22 June 2017; Received in revised form 8 March 2018; Accepted 10 March 2018
Available online 14 March 2018

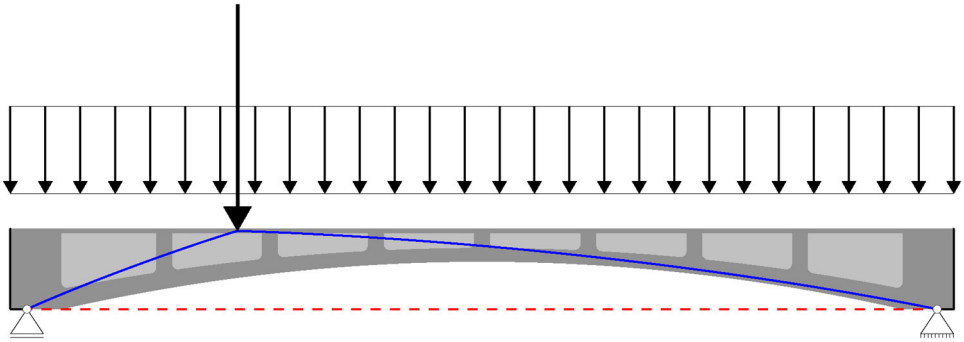

Fig. 1. The longitudinal section of a rib-stiffened floor shows the internal thrust lines (solid) terminating at supports and generating horizontal forces, which can be taken either by ties (dashed) or horizontal restraints.

2. Form and fabrication

The three prototypes discussed throughout this paper were produced using an ExOne S-Max 3D sand printer with a build volume of $1.8 \times 1.0 \times 0.7\,m^3$. The restricted build volume and structural segmentation pattern determined the maximum size and shape of the individual segments used in each floor (Fig. 2). No mechanical connection was used between neighbouring elements. Instead, the compression-dominant structural shape of the prototypes allowed for a simple interface design using only male–female interlocking features to guarantee alignment.

The form-finding process to generate the global compression-only shell geometry of the prototypes utilised Thrust Network Analysis (TNA) [12] and its software implementation RhinoVAULT [13,14]. Custom software extensions allowed quick iterations over different rib-pattern variations and alternatives, considering structural constraints such as well balanced force distributions (defined minimum and maximum axial force magnitudes in the ribs) and fabrication constrains such a minimum rib thicknesses and minimum spacing between neighbouring ribs (Fig. 3).

The relevant data of the optimised form-found geometry of the floor shells, the rib patterns, and the assumed force magnitudes for a defined design load, were all fed into a parametric low-poly mesh model, taking into consideration fabrication constraints such as the minimum structural thickness and maximum element size that would guarantee a good printing outcome using the selected sand printer and material. The parametric model was set-up using custom software tools utilising the computational framework *compas* [15], to control and visualise all relevant structural and geometrical data in real time, as well as to refine the print geometry using specifically developed mesh subdivision techniques. Three different floor geometries were generated for subsequent fabrication and testing (Fig. 4).

Depending on the length of the ribs and their assumed maximum internal compressive forces, individual thicknesses ranging between 8–35 mm were automatically assigned to the low-poly parametric mesh model. Furthermore, mesh edges and vertices were added parametrically in locations close to corner details to control their rounding-off radii for improved force distributions within the structure. Special rules were applied to rib corners adjacent to interfaces to distribute contact forces between neighbouring elements as uniformly as possible. The low-poly meshes for all elements were subsequently refined using constraint Catmull-Clark subdivision, resulting in solid volume meshes for 3D printing.

All floors presented in this paper have the same overall dimensions of $2.0\,m \times 1.4\,m \times 0.16\,m$, follow the same global compression-only shell geometry, and have approximately the same volume (floor 1: $0.13024\,m^3$, floor 2: $0.148546\,m^3$, floor 3: $0.145825\,m^3$). Floor 1 and floor 2 feature the same rib pattern topology seen in Fig. 4a and b. They are distinguished only by their local rib thicknesses, which are increased by approximately 50% towards the centre of floor 2 based on the assessment of local spalling during the first structural test of floor 1 (see Section 4). The segmentation design of floor 1 and floor 2 was informed by the internal force flow and follows the structural principle of a three-hinged arch with interfaces between neighbouring elements aligned perpendicular to the assumed force flow. The discretisation of floor 3 is based on yield lines for a solid slab of uniform thickness, indicating lines of maximum moment for the applied loading (Fig. 4c). By discretising the floor geometries, typical wall-to-wall spans of over eight metres can be achieved with prefabricated 3D sand-printed modules of limited size.

3. Material

This research focused on the use of industrial 3D printing using sand bonded by phenolic binders, which is characterised by its high printing precision, wide geometric freedom and facilitates the production of sufficiently strong and large parts [16,17] (ExOne GmbH, 2017; Voxeljet AG, 2017).

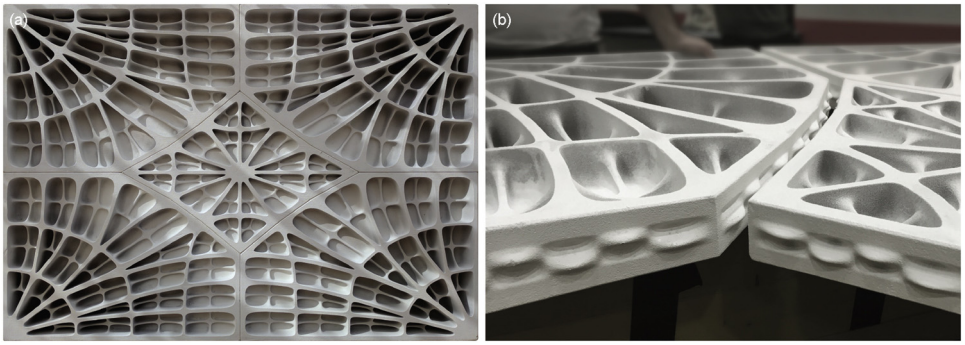

Fig. 2. (a) Top view of the first floor prototype (floor 1) consisting of five discrete parts. (b) The male–female interlocking features at the interfaces guaranteed proper alignment between neighbouring parts.

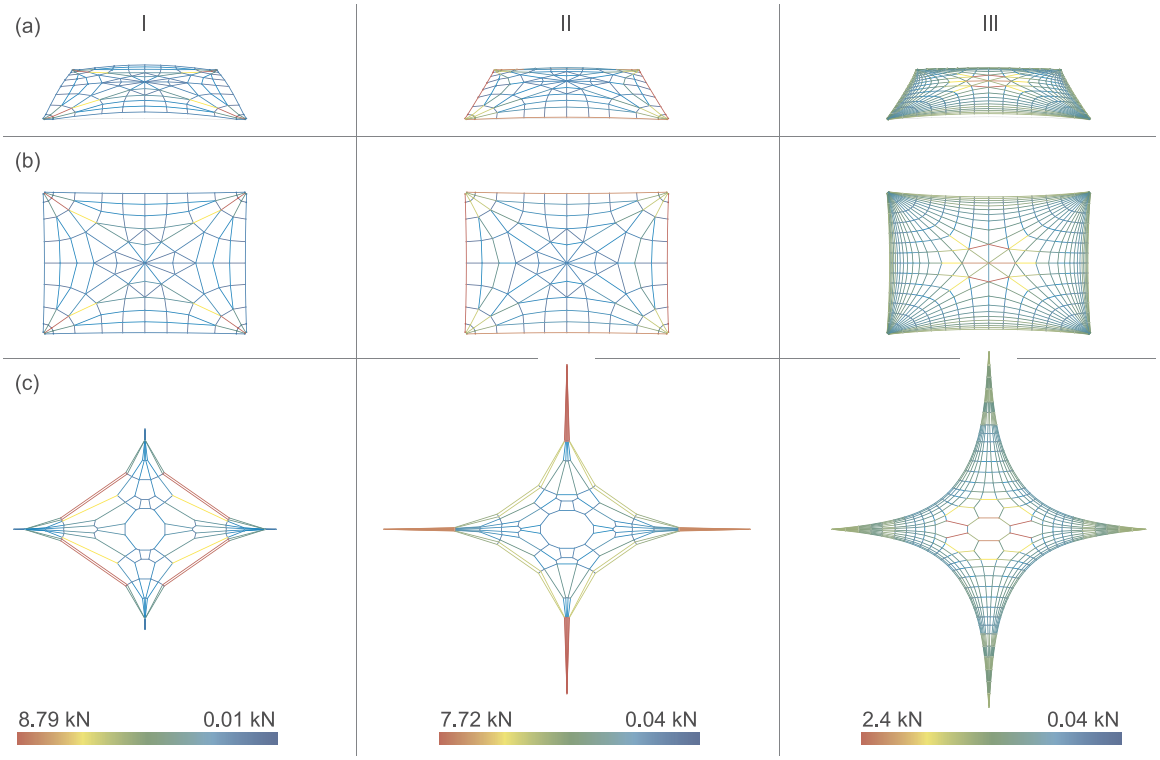

Fig. 3. TNA form-finding examples for (a) three possible compression-only shell geometries (b) layouts of forces (rib patterns) and (c) force distributions. Several hundred patterns and force distributions were tested using a custom software setup. Solution I represents the final pattern that was used for floor 1.

The sand is silica based, sized of the order of 100–200 μm, which is layered with an accuracy of 0.2% of the layer thickness. Elements can be produced with a tolerance of ± 0.3 mm. A resin binder is used with a sprayed epoxy coating on the outer surface, giving a material with a density of around 1300 kg/m^3. The epoxy coating penetrates the pores of the printed sand 5–10 mm and also adds significant strength, especially in tension, as the base sand material crumbles very easily with even manual handling.

Compression tests on small printed cylindrical samples showed that the uncoated sand has a compression strength between 4.0–5.5 MPa and a tensile strength between 1.4–1.8 MPa. The epoxy coated samples with significant infiltration reached beyond 12 MPa in compression and 5.5 MPa in tension. Due to the printing process, the material is slightly weaker in the vertical direction relative to the printing bed, due to the layering process. The Young's modulus of the uncoated samples was found to vary between 670–800 MPa (z direction), 820–940 MPa (x and y directions), with an increase to 1750–2250 MPa when epoxy saturated.

4. Load testing

To determine the strength and stiffness of the floor elements, the prototypes were tested against design code load levels and criteria, to observe the load–displacement and failure behaviour.

For the 2.8 m^2 plan area of the floors, an unfactored dead load of 1.0 kN/m^2 and live load of 2.0 kN/m^2 were simulated in a four-point bending test setup. The steel testing frame and experimental procedure used, was similar to that implemented for the fibre-reinforced concrete floor described in [4]. The key components of this test rig (Fig. 5) are: (1) 20 mm thick plated steel corner angles, bolted into the test frame with M20 bolts, (2) twin loading jacks in a closed oil-hydraulic system, applying loads via spreader beams to distribute the load across the floor width, (3) load cells underneath the jacks to measure the applied force, (4) displacement transducers attached to the topsides of floors to measure vertical displacements, (5) M12 steel (grade S460) ties with turnbuckles and inline 50 kN load cells for the testing of floor 3. Floors 1 and 2 were not pre-loaded with initial force, while floor 3 was pre-loaded with 3.5–5.0 kN in each tie.

To examine the behaviour of the floors under service loading, cyclic loading at different load levels of 20%, 40%, 50%, 60%, 80% and 100% of the design service loading were applied, was then followed by a 24 h 100% sustained loading period according to [18]. The results showed the maximum deflections were 12.4 mm for floor 1, 9.6 mm for floor 2, and 14.5 mm for floor 3. Due to hinging that formed at the interfaces between the discrete components, deflections increased, and were larger than typical span/250 limits by 20–80%.

For ultimate load testing, the applied force was increased until the peak load, and then continued into the unloading stage. For floors 1 and 2, distinct peak loads of 14.0 kN and 17.6 kN were found, while the testing of floor 3 was halted at 18.8 kN, to keep the horizontal forces in the ties safely below their design yield load. For floors 2 and 3, these loads are above those needed for design using a dead load safety factor of 1.35 and a live load factor of 1.5, while floor 1 was just shy of this load by 0.46 kN (3%).

Failure of the floors initiated with cracks propagating across the width on the underside, combined with crushing and spalling of the material on the topside (Fig. 6). From the side, significant hinging was observed with increased vertical displacements. From the observations on how floor 1 collapsed, in particular the areas in which material locally failed, additional rib thickness was given to the design of floor 2. The geometry improvements from floor 1 to floor 2 are evidenced by the additional 3.6 kN of load carrying capacity.

From the initial gradients of the force–displacement curves in Fig. 7, it is clear that floors 1 and 2 with the clamped corner supports, were stiffer against vertical deflections than floor 3 which was pre-loaded with tie supports. Significantly more hinging and deflections was witnessed for floor 1 than floor 2, associated with an improved interface design in floor 2. There was no observable cracking or local failure of floor 3 when the test was terminated.

For floor 3, each of the four sides had two steel ties and load cells

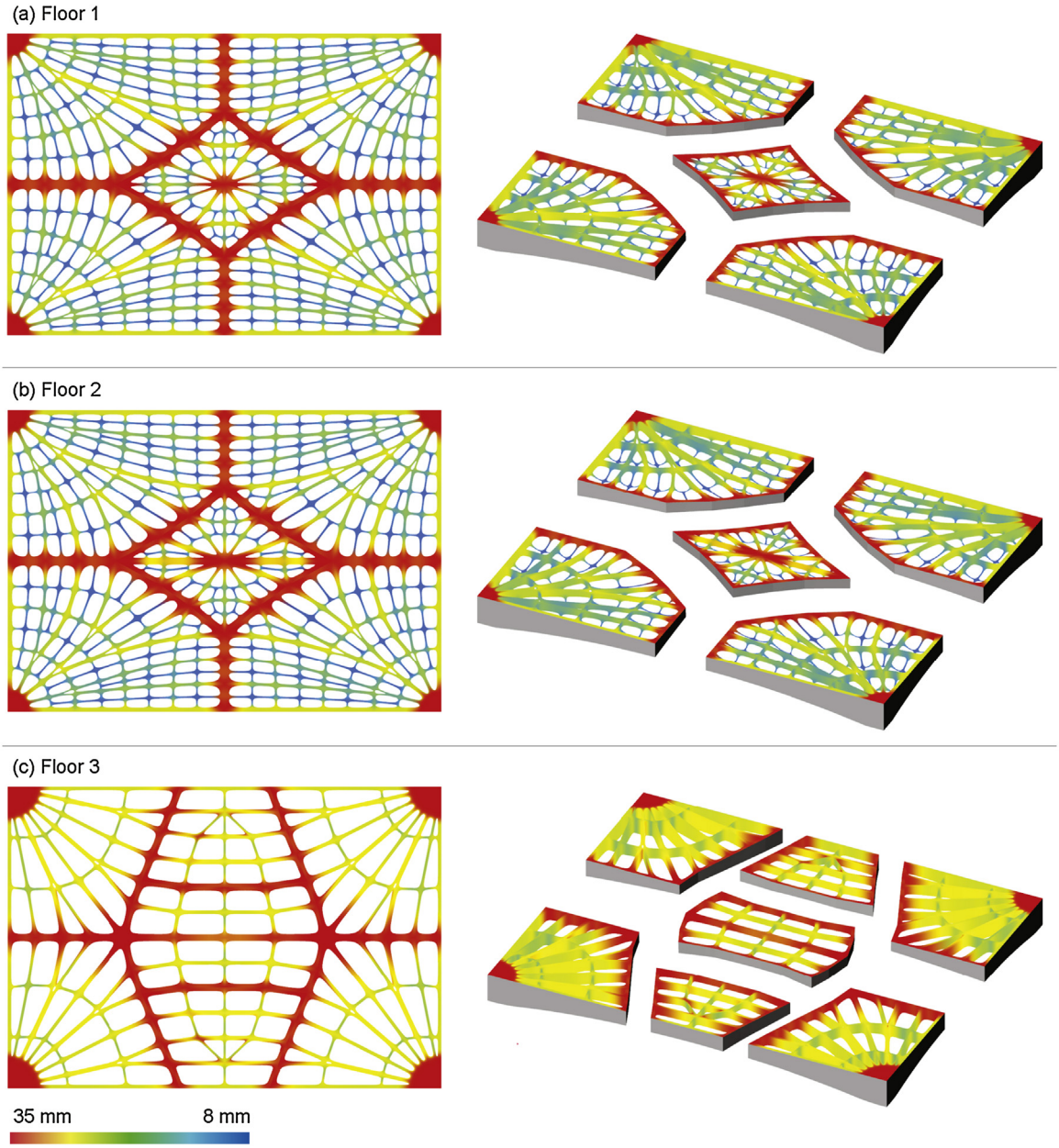

Fig. 4. Rib pattern geometries and discretisation layouts for (a) floor 1, (b) floor 2 and (c) floor 3. Differences between the floors include (a, b) local rib thicknesses (c) discretisation layouts.

connecting the corner plates to act as the internal restraint for the horizontal thrust forces. The variation of tie loads as measured by the load cells is plotted in Fig. 8, grouping the curves into pairs depending on whether the tie was the upper or lower element of each side, and for the longer or shorter spans of the floor. The lower ties took increasing load as the external forces increased to just below 20 kN. This was also true for the short-span upper ties, while the upper ties of the long-span continuously decreased and eventually became slack, indicating that all horizontal thrust was taken by the lower ties. As the M12 ties had a design yield load of 35 kN, the testing of floor 3 was halted when the tie force in one of the lower long-span ties reached 30 kN. The tie system had no detrimental effect on the load carrying capacity, but increased deflections when compared to the fixed corner cases, however this could be eliminated with increased pre-loading, taking care not to overstress the material in compression.

5. Environmental impact

Nearly 40% of the world's energy consumption and one third of related global greenhouse gas (GHG) emissions are attributable to the building sector [19]. Significant research and legislative efforts have been made to reduce GHG emissions during the operation of the building (operational emissions), while the emissions produced during construction (embodied emissions) have received far less attention. Recently, increased focus has been directed at embodied emissions, since these have been found to represent a large percentage of the total building lifecycle GHG emissions; this percentage will increase as buildings become more energy-efficient during their operation [19]. There are two ways to reduce embodied GHG emissions: (i) by reducing the volume of materials used and (ii) by utilising low embodied-carbon materials [3]. It has also been emphasised recently that the highest portion of embodied emissions relates to the structure of buildings [20] and in particular to floor and roof slabs [3,21].

Fig. 5. The steel testing frame used to load the floor elements in a four-point bending configuration.

This research addresses primarily the reduction of embodied GHG emissions by demonstrating the feasibility of a new structural floor system that reduces material consumption by as much as 70% when compared to conventional solid concrete floor slabs [22]. Additionally, the reduction of weight per floor has a significant effect on the weight of the overall structure, in particular for highrise buildings, and thus the size of its foundations. Furthermore, the cavities created by omitting material can be used to integrate building systems within the slab, rather than layering them above or below the floor, resulting in the gain of almost one extra storey for every three floor levels [23].

To date, no reliable data could be found regarding the embodied GHG emissions of the utilised 3D sand-printed material. The current recycling of 3D sand-printed structures is difficult due to issues with material separation at the end of their life cycles [24]. A potential solution for this issue can be found in the literature, discussing methods to replace phenolic resins with inorganic binder materials to reduce emissions in the recycling process of 3D sand-printed structures [25], which could significantly improve the overall sustainability of 3D sand-printed building components.

However, and more importantly, we consider the structurally weak sand-printed material as a placeholder for “new”, low-embodied energy materials, such as concrete based on alkali-activated cements (AAC) based on recycled waste [26] that are suited to be used in 3D-printing and alternative digital fabrication processes [27]. These recyclable and environmentally friendly materials typically have lower strength than commonly used engineering materials such as ordinary Portland cement (OPC). With the prototypes described in this paper, we have demonstrated that sufficient load-bearing capacity can come through structural geometry rather than material strength, providing a solution for such materials to be used structurally and safely, thus directly addressing the second recommendation on utilising low embodied-carbon materials given in [3].

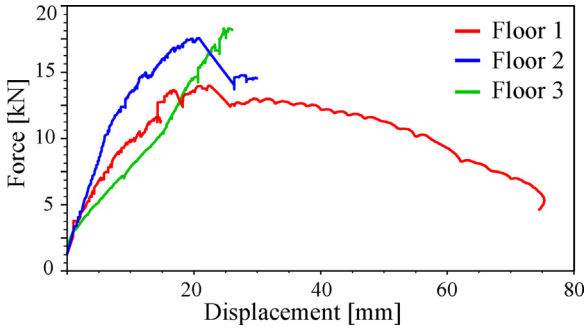

Fig. 7. Applied force–vertical displacement plots for the three 3D printed floors. Note that the ultimate load was not reached for floor 3.

6. Conclusions

This research utilised 3D printed sand as a structural medium to create unreinforced structural floor elements. The weak tensile material properties inspired compression dominated geometries, designed through form-finding with Thrust Network Analysis and RhinoVAULT. The digital design tools combined with the rapid fabrication speed of 3D printing, allowed many variations to be designed, for which three were physically realised and subsequently tested. Limits on the size of the printing bed, forced the floors to be discretised into separate parts, and then tested after assembling them together. The discretisation makes regions of the structure that would normally generate bending

Fig. 6. The compressive stresses on the topside of the floors, caused localised cracking and spalling of the printed sand, leading to failure.

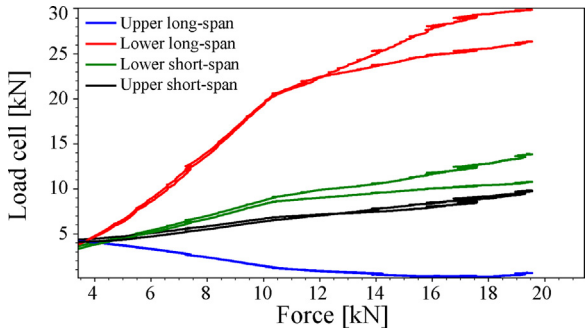

Fig. 8. Internal tie loads versus total external applied force for the third 3D printed floor.

moments, to be pre-cracked or pre-hinged, thus forcing the structure to be tension free at these locations. The concept is similar to a three-pinned arch, where the introduction of a hinge reduces the statical indeterminacy.

All floors were load tested to understand their behaviour under typical service and ultimate loading conditions, and with different support conditions and pre-load. The cyclic and sustained loading showed the floors could withstand typical service loading, albeit with slightly higher deflections than would be expected by design codes. Further loading to ultimate limit state levels showed a failure mechanism consisting of cracking on the floor underside and crushing/spalling on the topside. The floors with fixed corner supports were stiffest, while the floor with steel tie restraint system and initial pre-load was able to take the highest load. Plots of the tensile forces in the ties provided an insight into how the tie forces changed as the applied loading was increased.

By capitalising on the short time from making observations during testing, designing a new floor with the developed computational framework, and then 3D printing the new geometry, we were able to incrementally and rapidly improve the designs with each iteration. These improvements were with respect to the discretisation pattern, structural sizing of ribs and the component interfaces, which led to successively enhanced floors that were able to take further loading or deflect less.

Finally, we have provided insights regarding the potential to significantly lower the environmental impact of building structures through the use of 3D-printed floors as presented in this paper.

Acknowledgements

The authors would like to thank Ursula Frick for assistance with the 3D mesh modelling process and Alessandro Dell'Endice for assistance with the set-up and testing of the floors, Heinz Richner from the Institut für Baustoffe (IfB) at ETH Zurich for the material testing, and Dominik Werne from the Institut für Baustatik und Konstruktion (IBK) at ETH Zurich for the testing rig of the prototype floor. This research was partially supported by the Swiss National Science Foundation through the National Centre of Competence in Research (NCCR) Digital Fabrication (Agreement #51NF40-141853).

References

[1] J. Ochsendorf, M. Freeman, Guastavino Vaulting: The Art of Structural Tile, Princeton Architectural Press, Princeton, 2013.
[2] World Business Council for Sustainable Development, The Cement Sustainability Initiative: Our Agenda for Action. Technical Report, WBCSD, 2002.
[3] C. De Wolf, M. Ramage, J. Ochsendorf, Low carbon vaulted masonry structures, J. Int. Assoc. Shell Spat. Struct. (J. IASS) 57 (04 December) (2016) 275–284.
[4] A. Liew, D. López López, T. Van Mele, P. Block, Design, fabrication and testing of a prototype, thin-vaulted, unreinforced concrete floor, Eng. Struct. 137 (2017) 323–335.
[5] J. Pegna, Exploratory investigation of solid freeform construction, Autom. Constr. 5 (5) (1997) 427–437.
[6] B. Dillenburger, M. Hansmeyer, Printing architecture: castles made of sand, in: Fabio Gramazio, Matthias Kohler, Silke Langenberg (Eds.), Fabricate: Negotiating Design and Making, Zurich, 2013, pp. 92–97 gta Verlag.
[7] A.G. Voxeljet, Voxeljet Architecture, (2017) (accessed 01.06.17), http://www.voxeljet.com/industries/architecture/.
[8] B. Khoshnevis, Automated construction by contour crafting-related robotics and information technologies, Autom. Constr. 13 (1) (2004) 5–19.
[9] S. Lim, R.A. Buswell, T.T. Le, S.A. Austin, A.G.F. Gibb, T. Thorpe, Developments in construction-scale additive manufacturing processes, Autom. Constr. 21 (2012) 262–268.
[10] T.T. Le, S.A. Austin, S. Lim, R.A. Buswell, R. Law, A.G.F. Gibb, T. Thorpe, Cement and concrete research hardened properties of high-performance printing concrete, Cem. Concr. Res. J. 42 (2012) 558–566.
[11] C. Gosselin, R. Duballet, P. Roux, N. Gaudillière, J. Dirrenberger, P. Morel, Large-scale 3D printing of ultra-high performance concrete – a new processing route for architects and builders, JMADE 100 (2016) 102–109.
[12] P. Block, J. Ochsendorf, Thrust network analysis: a new methodology for three-dimensional equilibrium, J. Int. Assoc. Shell Spat. Struct. 48 (3) (2007) 1–8.
[13] M. Rippmann, L. Lachauer, P. Block, Interactive vault design, Int. J. Space Struct. 27 (4) (2012) 219–230.
[14] M. Rippmann, Funicular Shell Design: Geometric Approaches to Form Finding and Fabrication of Discrete Funicular Structures. PhD Thesis, ETH-Zürich, 2016.
[15] T. Van Mele, A. Liewe, T. Mendez, M. Rippmann, COMPAS: A Framework for Computational Research in Architecture and Structures, (2017) (in preparation), https://compas-dev.github.io.
[16] ExOne GmbH, ExOne 3D Printing Systems, (2017) (accessed 01.06.17), http://www.exone.com/Systems/.
[17] A.G. Voxeljet, Voxeljet 3D Printing Systems, (2017) (accessed 01.06.17), http://www.voxeljet.com/3d-printing-system/.
[18] A.C.I. Committee, 437R-03: Strength Evaluation of Existing Concrete Buildings, Committee Report 437 (2003), pp. 1–28.
[19] T. Ibn-Mohammed, R. Greenough, S. Taylor, L. Ozawa-Meida, A. Acquaye, Operational vs. embodied emissions in buildings – a review of current trends, Energy Build. 66 (2013) 232–245.
[20] Catherine De Wolf, Low Carbon Pathways for Structural Design: Embodied Life Cycle Impacts of Building Structures. PhD Thesis, Massachusetts Institute of Technology, 2017.
[21] N. Huberman, D. Pearlmutter, E. Gal, I.A. Meir, Optimizing structural roof form for life-cycle energy efficiency, Energy Build. 104 (2015) 336–349.
[22] Isolda Agustí-Juan, Guillaume Habert, Environmental design guidelines for digital fabrication, J. Clean. Prod. 142 (2017) 2780–2791.
[23] Arno Schlueter, Adam Rysanek, Clayton Miller, Jovan Pantelic, Forrest Meggers, Matthias Mast, Marcel Bruelisauer, Chen Kian Wee, 3for2. Realizing spatial, material, and energy savings through integrated design, J. Council Tall Build. Urban Habitat (2) (2016) 40–45.
[24] I. Agustí-Juan, S. Zingg, G. Habert, End-of-Life consideration for hybrid material systems, Proceedings of the 14th International Conference on Durability of Building Materials and Components Gent, Belgium, 2017.
[25] M. Xia, J. Sanjayan, Method of formulating geopolymer for 3d printing for construction applications, Mater. Des. 110 (2016) 382–390.
[26] P. Van den Heede, N. De Belie, Environmental impact and life cycle assessment (LCA) of traditional and 'green' concretes: literature review and theoretical calculations, Cem. Concr. Compos. 34 (4) (2012) 431–442.
[27] Timothy Wangler, Ena Lloret, Lex Reiter, Norman Hack, Fabio Gramazio, Matthias Kohler, Mathias Bernhard, Benjamin Dillenburger, Jonas Buchli, Nicolas Roussel, Robert Flatt, Digital concrete: opportunities and challenges, RILEM Tech. Lett. 1 (2016) 67–75.